Electronic supplementary information

Tetrakaidecahedron-shaped Cu four-core supramolecular as novel high-performance electrode material for lithium-ion batteries

Xueli Chen,[a] Kongyao Chen,*[a] Gaojie Li,[a] Chao Huang,[a] Yingying Zhang,[a] Yanling Feng,[a] Na Qin,[a] Jiahuan Luo,[c] Weihua Chen[b] and Liwei Mi*[a]

[a] Center for Advanced Materials Research, Zhongyuan University of Technology, Zhengzhou 450007, P. R. China

[b] College of Chemistry and Molecular Engineering, Zhengzhou University, Zhengzhou 450001, P. R. China

[c] Department of Chemical and Environmental Engineering, Anyang Institute of Technology, Anyang, 455000, P. R. China

*Corresponding author.

E-mail address: chenkongyao@zut.edu.cn, mlwzzu@163.com.

1. Experimental Section

1.1. Sample preparation

Cu-FCS was prepared by one-pot solvothermal reaction. Typically, 0.21 g $CuCl_2 \cdot 2H_2O$ was dissolved in 20 mL methanol, and 0.12 mL pyridine-3-carbaldehyde were added to the above solution, then 6 drops dichloromethane were added. The above solution was stirred and transferred to a 30 mL Teflon-sealed autoclave, then the autoclave was heated to 70°C and kept for 6 days. Finally a brown product was obtained.

1.2. Crystal data collection and refinement

The crystal data of Cu-FCS was attained by a Bruker D8 VENTURE diffractometer (λ=0.71073 Å, Mo-Kα). The SAINT and SADABS program were carried out to control the restoring data and semiempirical absorption correction. The structure of Cu-FCS was carried out, and the structure formula is [$Cu_4(L)_4(\mu_4\text{-}O)Cl_6$ L = pyridine-3-carbaldehyde]. The molecular formula is ($C_{24}H_{20}Cl_6Cu_4N_4O_5$). Detailed crystallographic data was displayed in **Table S1**.

1.3. Characterizations

Power X-ray diffraction (XRD) patterns were obtained by an X-ray powder diffractometer (Rigaku Ultima IV, Japan) using Cu-Kα radiation with a scan rate of 10° min^{-1}. The morphology was characterized by a scanning electron microscope (SEM, Zeiss Merlin Compact, Germany) equipped with an energy dispersive X-ray spectroscopy (EDS) system. Fourier transform infrared spectroscopy (FT-IR) was displayed by a spectrometer (NicoletiS50, Thermo scientific) at room temperature. Cu-FCS was mixed with KBr at a weight ratio of 1:100, and the scan range is 400-4000 cm^{-1}. Thermogravimetric analysis (TG) were characterized in N_2 atmosphere from 50°C to 800°C with a heating rate of 10°C min^{-1} (NETZSCH TG209F1, Germany). X-ray photoelectron spectroscopy (XPS) analysis was performed by an energy spectrometer (Thermoscientific K-Alpha).

The chemical composition is measured by FT-IR (Fig. S2). The peak at 572 cm^{-1} may belongs to Cu-O.[1] The peak at 1475 cm^{-1}, 1449 cm^{-1}, 1427 cm^{-1} belongs to pyridine rings.[2] The strong characteristic peak at 1612 cm^{-1} may belong to asymmetric and symmetric stretching vibrations of C=O and C=N. Generally speaking, the chemical composition of Cu-FCCS coincides with its molecular formula.

According to the survey spectrum, the peaks prove the presence of Cu2p, C1s, N1s, O1s and Cl1s. In detail, the peaks at 952.5 eV and 932.7 eV can be attributed to Cu $2p_{1/2}$ and Cu $2p_{3/2}$ of Cu^{2+}, which demonstrates the valence of Cu in Cu-FCS.[3] Similarly, the XPS spectrum of C can be divided into three peaks. The peak at 284.8 eV belongs to C-C bond of aldehyde group, the peak at 285.8 eV belongs to C-N bond in aldehyde group, and the peak at 288.1 eV belongs to C=O bond.[4, 5] Besides, the peak at 400.0 eV belongs to C-N bond in pyridine ring, the peak at 532.3 eV belongs to Cu-O bond in Cu clusters, and the peaks at 198.4 eV and 199.9 eV belong to Cu-Cl bond in Cu clusters, respectively.[6, 7]

when act as electrode materials for LIBs, thermal stabilities are very important for the application of supramoleculars, so the thermal stability of Cu-FCS is measured by TG (Fig. 1f). At first, no obvious mass loss is detected below 200°C, manifesting a good thermal stability of Cu-FCS. The following mass loss (55 wt%) from 200°C to 258°C may be attributed to the decomposition of organic ligands, and the mass loss (30 wt%) from 258°C to 640°C may be attributed to the further decomposition of Cu compounds.

1.4. Electrochemical measurements

70 wt% Cu-FCS, 20 wt% acetylene black and 10 wt% polyvinyidenefluorate (PVDF) in N-methyl pyrrolidone (NMP) was mixed and ball-milled for 10 h, and the particle size Cu-FCS will be reduced to hundreds of nanometers. Then the slurry was coated on a Cu foil. The above foil was dried at 80°C for 12 h in vacuum drying oven, and punched into discs with diameters of 8 mm. The mass loading of Cu-FCS was 2~3 mg cm^{-2}. Coin cells were assembled in an Ar-filled glovebox. For LIBs, Li foils were used as counter electrodes, 1 mol L^{-1} LiPF$_6$ in ethylene carbonate/dimethyl carbonate/diethyl carbonate (EC/DMC/DEC 1:1:1 in volume) was used as the electrolyte, and Celgard 2400 films were used as separators. The cycling and rate performance were measured by a battery test system (CT 2001A, Land, Wuhan). The cyclic voltammetry (CV) test was performed by an electrochemistry workstation (Chenhua CHI660e, Shanghai) with a voltage range of 0.2~3.0 V. The electrochemical impedance spectra (EIS) were measured with a frequency range from 0.1 Hz to 100 kHz.

Some Cu-FCS crystals are milled into powder and weighed (m_{Cu-FCS}). Then the powder is put into a measuring cylinder and dropped from a certain height to the tabletop. The above steps are repeated several times until the volume no longer decreases, then the volume is achieved (V_{Cu-FCS}). The tap density of the powder is calculated from the mass and volume (ρ_{Cu-FCS}=1.43±0.05 g cm-3). After the cycle test, the mass capacity (C_m) of Cu-FCS is achieved, and the volume specific capacity can be achieved according to the formula $C_V=C_m*\rho_{Cu-FCS}$.
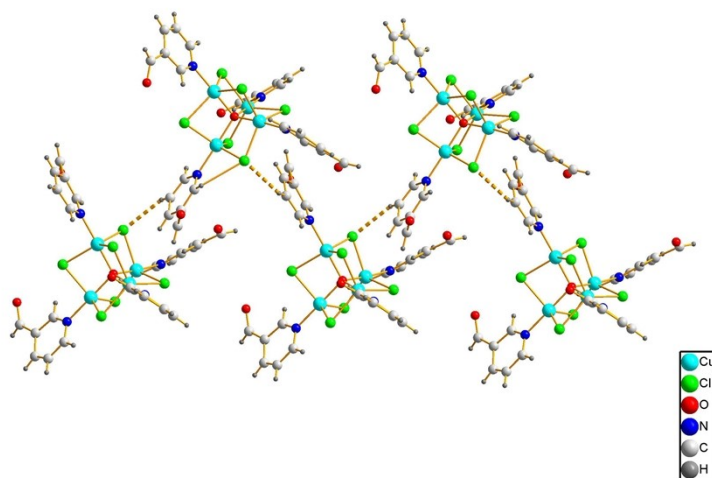
Fig. S1 The stacking structure of Cu-FCS.
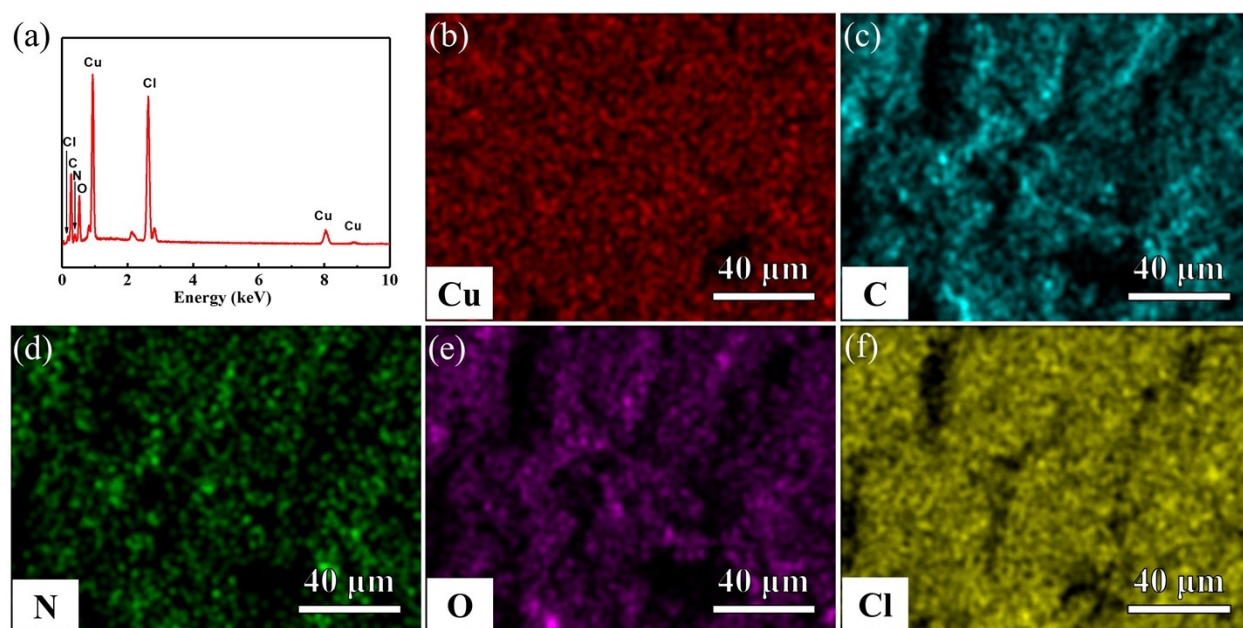
Fig. S2 (a) EDS result of Cu-FCS. Element mapping of (b) Cu, (c) C, (d) N, (e) O and (f) Cl.
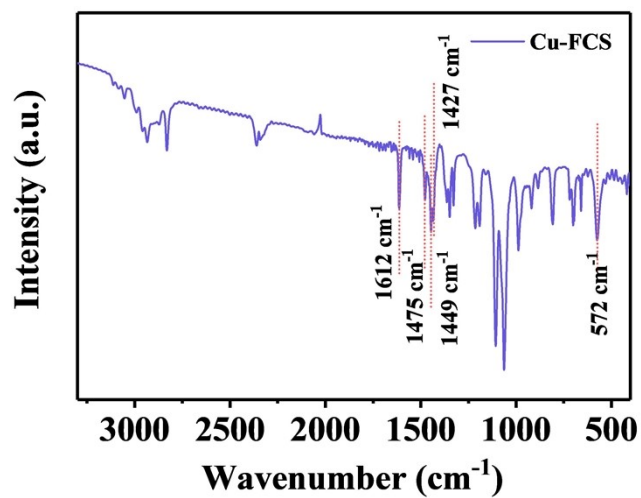
Figure S3 FT-IR spectra of Cu-FCS.
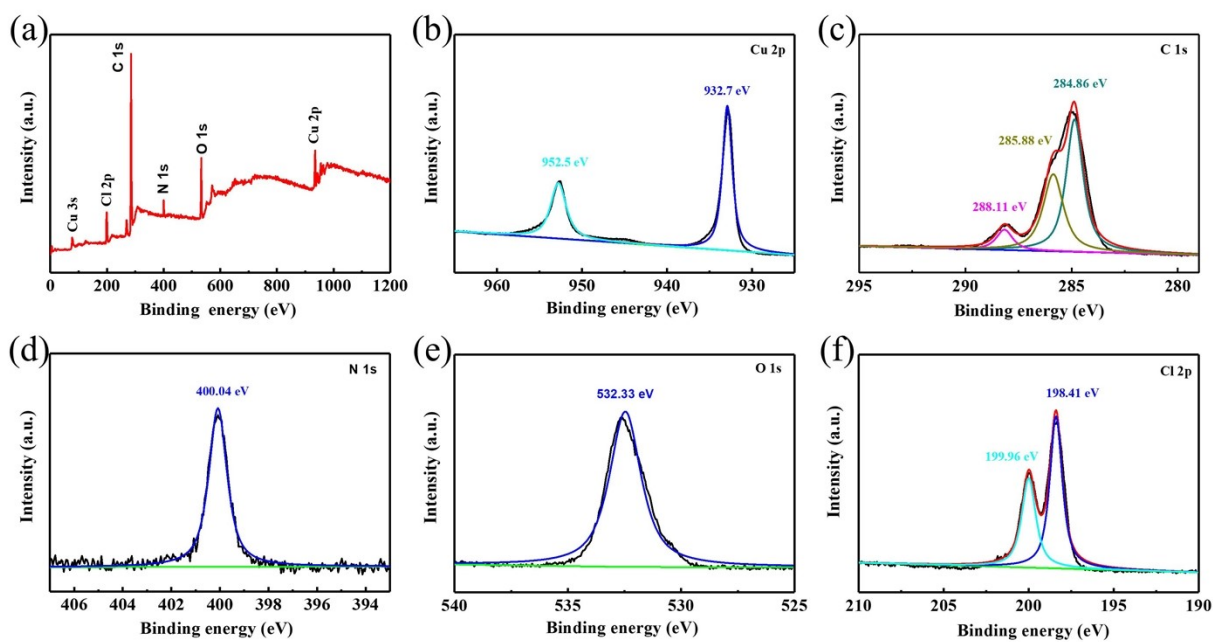
Fig. S4 (a) XPS survey spectra of Cu-FCS. High-resolution XPS spectrums of (b) Cu, (c) C, (d) N, (e) O and (f) Cl.
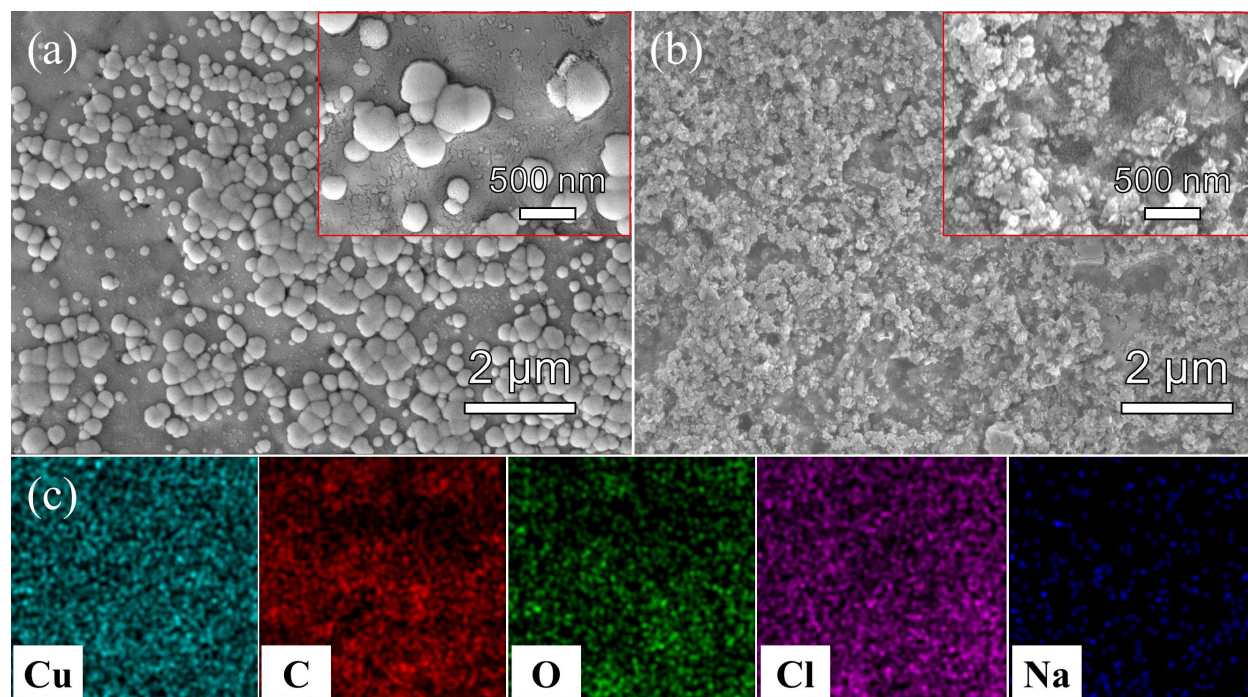
Fig. S5 (a) The morphology of pristine Cu-FCS electrode. (b) The morphology of Cu-FCS electrode after cycle test. (c) Element distribution of Cu-FCS electrode after cycle test.

Table S1. Crystal datas and structural refinement parameters of Cu-FCS.

	Cu-FCS
Formula	$C_{24}H_{20}$ $Cl_6N_4Cu_4O_5$
	911.30
T / K	293
λ / Å	0.71073
Crystal system	Monoclinic
Space group	$P2_1/c$
a / Å	12.709 (9)
b / Å	12.889 (9)
c / Å	13.598 (8)
α / deg	90
β / deg	91.23(2)
γ / deg	90
V / Å^3	2227 (2)
Z	2
ρ_{calc} / g cm^{-3}	1.359
μ / mm^{-1}	2.274
Reflections collected	8286
Independent reflections	7831
R(int)	0.0275
ϑ range / deg	2.18 to 25.5
F(000)	900
GOF on F^2	1.060
R_1 / wR_2 [$I > 2\sigma(I)$]	0.0581 / 0.1807
R_1 / wR_2 (all data)	0.0606 / 0.1860

a$R1 = \sum||F0| - |Fc||/\sum|F0|$. b$wR_2 = [\sum w(F_0^2 - F_c^2)^2/\sum w(F_0^2)^2]^{1/2}$.

Table S2. Selected bond lengths (Å) and angles (º) of Cu-FCS.

		Cu-FCS			
Cu1-O1	1.910(6)	N2-Cu1-Cl4	95.0(3)	Cl3-Cu3-Cl5	119.51(12)
Cu1-N2	2.007(9)	Cl5-Cu1-Cl4	124.46(12)	Cl2-Cu3-Cl5	116.02(13)
Cu1-Cl5	2.388(3)	O1-Cu1-Cl1	84.5(2)	O1-Cu4-N3C	175.4(3)
Cu1-Cl4	2.404(3)	N2-Cu1-Cl1	96.2(3)	O1-Cu4-Cl1	85.59(19)
Cu1-Cl1	2.424(3)	Cl5-Cu1-Cl1	113.99(12)	N3C-Cu4-Cl1	91.2(3)
Cu2-O1	1.908(6)	Cl4-Cu1-Cl1	119.30(12)	O1-Cu4-Cl2	85.36(19)
Cu2-N1	1.986(9)	O1-Cu2-N1	177.9(4)	N3C-Cu4-Cl2	99.1(3)
Cu2-Cl6A	2.365(3)	O1-Cu2-Cl6A	85.6 (2)	Cl1-Cu4-Cl2	121.32(12)
Cu2-Cl3	2.400(3)	N1-Cu2-Cl6A	95.8(3)	O1-Cu4-Cl6A	83.7(2)
Cu2-Cl4	2.450(3)	O1-Cu2-Cl3	84.8 (2)	N3C-Cu4-Cl6A	95.2(3)
Cu3-O1	1.902(6)	N1-Cu2-Cl3	93.1(3)	Cl1-Cu4-Cl6A	121.26(12)
Cu3-N4	1.994(9)	Cl6A-Cu2-Cl3	123.12(13)	Cl2-Cu4-Cl6A	115.08(13)
Cu3-Cl3	2.403(3)	O1-Cu2-Cl4	83.70(18)	Cu4-Cl1-Cu1	80.78(9)
Cu3-Cl2	2.416(3)	N1-Cu2-Cl4	96.8(3)	Cu4-Cl2-Cu3	80.67(10)
Cu3-Cl5	2.426(3)	Cl6A-Cu2-Cl4	120.65(13)	Cu2-Cl3-Cu3	80.64(9)
Cu4-O1	1.914(6)	Cl3-Cu2-Cl4	113.73(12)	Cu1-Cl4-Cu2	80.65(9)
Cu4-N3C	1.967(9)	O1-Cu3-N4	179.3(4)	Cu1-Cl5-Cu3	80.36(10)
Cu4-Cl1	2.383(3)	O1-Cu3-Cl3	84.8(2)	Cu2-Cl6A-Cu4	81.18(10)
Cu4-Cl2	2.387(3)	N4-Cu3-Cl3	95.8(3)	Cu3-O1-Cu1	109.1(3)
Cu4-Cl6A	2.439(3)	O1-Cu3-Cl2	84.8(2)	Cu3-O1-Cu4	109.1(3)
O1-Cu1-N2	179.2 (4)	N4-Cu3-Cl2	95.1(3)	Cu1-O1-Cu4	109.1(3)
O1-Cu1-Cl5	85.6(2)	Cl3-Cu3-Cl2	121.99(12)	Cu3-O1-Cu2	109.3(3)
N2-Cu1-Cl5	93.9(3)	O1-Cu3-Cl5	84.7(2)	Cu1-O1-Cu2	110.7(3)
O1-Cu1-Cl4	84.91(19)	N4-Cu3-Cl5	94.8(3)	Cu4-O1-Cu2	109.4(3)

Symmetry transformations used to generate equivalent atoms in copper cluster: [1]+X,1/2-Y,-1/2+Z; [2]+X,1/2-Y,1/2+Z. **2**: [1]+X,3/2-Y,-1/2+Z; [2]+X,3/2-Y,1/2+Z.

Table S3. Electrochemical performance contrast between Cu-FCS and recent MOFs.

Samples	Specific capacity (mA h g^{-1})	Cycle (mA h g^{-1})	Rate (mA h g^{-1})	Voltage (V)	Ref.
[Co$_3$(L$_1$)(N$_3$)$_4$]	617.0 (100 mA g^{-1})	358.0 after 200 cycles (100 mA g^{-1})	346.0 (1000 mA g^{-1})	0.01~3.0	8
Ni-MOFs	842.0 (50 mA g^{-1})	620.0 after 100 cycles (100 mA g^{-1})	229.0 (1000 mA g^{-1})	0.01~3.0	9
NENU-507	767.0 (200 mA g^{-1})	640.0 after 100 cycles (100 mA g^{-1})	480.0 (500 mA g^{-1})	0.01~3.0	10
Cu$_3$(BET)$_2$	740.0 (96 mA g^{-1})	474.0 after 50 cycles (383 mA g^{-1})	644.0 (191 mA g^{-1})	0.05~3.0	3
[Ni(4,4'-bpy)(tfbdc)(H$_2$O)$_2$]	313.0 (100 mA g^{-1})	406.0 after 50 cycles (50 mA g^{-1})	108.0 (1000 mA g^{-1})	0.01~3.0	11
S-Co-MOF	1107.0 (100 mA g^{-1})	601.0 after 700 cycles (500 mA g^{-1})	604.0 (2000 mA g^{-1})	0.01~3.0	7
Mn-1,4-BDC@200	870.6 (100 mA g^{-1})	974.0 after 100 cycles (100 mA g^{-1})	435.0 (1000 mA g^{-1})	0.01~3.0	12
Co(L) MOF/RGO	1805.5 (100 mA g^{-1})	1185.0 after 50 cycles (100 mA g^{-1})	430.6 (2000 mA g^{-1})	0.01~3.0	13
Cu-FCS	1042.1 (100 mA g^{-1})	494.5 after 700 cycles (1000 m A g^{-1})	459.4 (2000 mA g^{-1})	0.20~3.0	This work

Table S4. Equivalent circuit fitting results of Cu-FCS in LIBs.

Name	Value (ohm)	Error (%)
Rs	1.818	3.46
Rct	173.800	2.96
W1-R	4895.000	1.58
W1-T	2.091	6.92
W1-P	0.705	0.85
CPE1-T	$1.982*10^{-5}$	11.81
CPE1-P	0.793	14.79

References

1 X. Wang, X. Lu, L. Wu and J. Chen, *Biosens. Bioelectron.*, 2015, **65**, 295-301.
2 M. Rehakova, L. Fortunova, Z. Bastl, S. Nagyova, S. Dolinska, V. Jorik and E. Jona, *J Hazard. Mater.*, 2011, **186**, 699-706.
3 S. Maiti, A. Pramanik, U. Manju and S. Mahanty, *Microporous Mesoporous Mater.*, 2016, **226**, 353-359.
4 J. Hao, Y. Wang, C. Chi, J. Wang, Q. Guo, Y. Yang, Y. Li, X. Liu and J. Zhao, *Sustain. Energ. Fuels*, 2018, **2**, 2358-2365.
5 J. Gu, Y. Gu and S. Yang, *Chem. Commun.*, 2017, **53**, 12642-12645.
6 X. Zheng, Y. Li, Y. Xu, Z. Hong and M. Wei, *CrystEngComm*, 2012, **14**, 2112.
7 C. Li, X. Hu, X. Lou, L. Zhang, Y. Wang, J. P. Amoureux, M. Shen, Q. Chen and B. Hu, *J. Mater. Chem. A*, 2016, **4**, 16245-16251.
8 T. Gong, X. Lou, E. Q. Gao and B. Hu, *ACS Appl. Mater. Interfaces*, 2017, **9**, 21839-21847.
9 Y. Zhang, Y. B. Niu, T. Liu, Y. T. Li, M. Q. Wang, J. Hou and M. Xu, *Mater. Lett.*, 2015, **161**, 712-715.
10 Y. Y. Wang, M. Zhang, S. L. Li, S. R. Zhang, W. Xie, J. S. Qin, Z. M. Su and Y. Q. Lan, *Chem. Commun.*, 2017, **53**, 5204-5207
11 C. Shi, X. Wang, Y. Gao, H. Rong, Y. Song, H. Liu and Q. Liu, *J. Solid State Electrochem.*, 2017, **21**, 2415-2423.
12 H. Hu, X. Lou, C. Li, X. Hu, T. Li, Q. Chen, M. Shen and B. Hu, *New J. Chem.*, 2016, **40**, 9746-9752.
13 C. Dong and L. Xu, *ACS Appl. Mater. Interfaces*, 2017, **9**, 7160-7168.